



HAL
open science

NO solubility in water and brine up to 60 MPa and 373 K by combining Raman spectroscopy and molecular simulation

Jérôme Sterpenich, Marie-Camille Caumon, Véronique Lachet, Benoit Creton,
Mohamed El Jarmouni, Aurélien Randi, Pascal Robert

► **To cite this version:**

Jérôme Sterpenich, Marie-Camille Caumon, Véronique Lachet, Benoit Creton, Mohamed El Jarmouni, et al.. NO solubility in water and brine up to 60 MPa and 373 K by combining Raman spectroscopy and molecular simulation. *Journal of Raman Spectroscopy*, In press, 53 (3), pp.645-653. 10.1002/jrs.6072 . hal-03121642

HAL Id: hal-03121642

<https://hal.science/hal-03121642>

Submitted on 27 Jan 2021

HAL is a multi-disciplinary open access archive for the deposit and dissemination of scientific research documents, whether they are published or not. The documents may come from teaching and research institutions in France or abroad, or from public or private research centers.

L'archive ouverte pluridisciplinaire **HAL**, est destinée au dépôt et à la diffusion de documents scientifiques de niveau recherche, publiés ou non, émanant des établissements d'enseignement et de recherche français ou étrangers, des laboratoires publics ou privés.

NO solubility in water and brine up to 60 MPa and 373 K by combining Raman spectroscopy and molecular simulation

Jérôme Sterpenich¹, Marie-Camille Caumon¹, Véronique Lachet², Benoit Creton², Mohamed El Jarmouni¹, Aurélien Randi¹, Pascal Robert¹

¹GeoRessources lab, CNRS-Université de Lorraine, BP70239, 54506 Vandœuvre-lès-Nancy, France

²IFP Energies nouvelles, 1 et 4 avenue de Bois-Préau, 92852 Rueil-Malmaison, France

Abstract

In the processes of Carbon Capture and Storage, sulphur and nitrogen oxides (SO_x and NO_x) would be possibly injected with CO₂ depending on the origin of CO₂. The thermodynamic properties of these gases in saline aquifer are poorly known. Solubility is one of the key parameter to be implemented in geochemical codes modeling long-term evolution of the aquifer after injection. The solubility of NO is known only at atmospheric pressure. In this study, the solubility of NO in water and NaCl solutions was measured by Raman spectroscopy in the ranges 295-373 K and 2-60 MPa using a High Pressure Optical Cell and after calibration on a few data from molecular simulations. The results show a decrease of solubility when temperature increases and when salinity increases. No modification of NO speciation was observed.

Keywords

Nitrogen monoxide, solubility, water, molecular simulation, high pressure

Introduction

In the context of Carbon Capture and Storage (CCS), the role of impurities likely injected with CO₂ has to be tackled in order to assess the long term behaviour of the storage^[1-7]. As a function of the industrial process releasing CO₂ in the fumes (power plant, cement plant, glass industry...) and depending on the capture and purification processes, the composition of the CO₂-rich stream injected in geological storages can vary significantly. If gases such as Argon or Nitrogen can dominate the composition of impurities, other gases such as SO_x or NO_x can be minor but can cause the system to be chemically reactive. In the presence of water such gases can dissolve and produce strong acids that could react with storage components, such as reservoir and caprock, or well materials (cement and steel casing). If the thermodynamics of CO₂ under the pressure and temperature conditions of a storage (>7.4 MPa and >304.25 K, over the critical point of CO₂) is well known, this is not the case for sulphur and nitrogen oxides (SO_x and NO_x where x stands for the stoichiometric coefficient). As an example, the solubility data for NO are sparse and only atmospheric pressure is documented^[8-12]. However the solubility data are essential for the use of

the geochemical codes in order to predict the physical-chemical evolution of the storage and the possible chemical reactions occurring between fluids and minerals^[3,13].

The High Pressure Optical Cell (HPOC) is an experimental device combining a silica microcapillary, a heating-cooling stage, a pressurization device and a Raman microspectrometer^[14,15]. The microcapillary is used as a sample cell whose pressure and temperature can be controlled accurately. As silica is transparent in the visible range, Raman spectra can be recorded through the capillary. This device has been widely used in a wide range of applications, mainly gas solubility^[16-18], gas diffusion in aqueous solutions^[19-21], gas phase composition and density^[22-26] or to follow reaction processes^[27]. Raman spectroscopy is a semi-quantitative technique that requires to calibrate the intensity of the signal to a standard. Previous studies of CO₂ or CH₄ solubilities were calibrated on well-established thermodynamic models and experimental data. Unfortunately there is neither data nor accurate thermodynamic models for NO solubility. This is also not possible to prepare standard solutions at known NO concentration as there is no stable salt species giving dissolved NO with a known equilibrium

constant. In some previous studies, a Hg-plug were used to put water and gas inside the capillary at room temperature and pressure. The number of moles of each species was evaluated by measuring volume and using densities at room $TP^{[28-30]}$. However, it was not possible to use the Hg-plug method in our lab because of safety policies regarding Hg. Moreover, this method is questionable with highly soluble gases at room temperature (SO_2 , H_2S , etc.) because the aqueous phase can contain a large amount of dissolved gas at room conditions, affecting liquid density and global molal composition.

In this study we propose an original combination of HPOC and Raman spectrometry with molecular simulation to determine NO solubility in water and 1M-NaCl solutions from 2 to 60 MPa and from room temperature to 373 K.

Material and methods

Pressurization device and Fused Silica Capillary

The determination of NO solubility was performed acquiring Raman spectra of aqueous solutions loaded in silica capillaries using the same device as in previous studies^[16,17,31,32]. The experiments were performed at 295 K, 298 K, 308 K, 323 K, 333 K, and 373 ± 0.1 K and pressures ranging from 1 to 30 MPa (up to 60 MPa at 295 K), using a High Pressure Optical Cell. Experiments were performed in pure water (deionized water, 18.2 M Ω .cm) and at 298 K, 323 K and 373 K in 1M-NaCl solutions. After burning the polyimide coating, one end of the Fused Silica Capillary (FSC) tube was welded. The FSC was then filled with water or NaCl solution. It was then connected to the stainless tube of a pressurization device using epoxy glue. The FSC was gently evacuated under vacuum to be purged from atmospheric gases. The FSC was then filled with NO and then closed with a valve. Finally, the FSC was connected to the High Pressure device. Pressure was controlled to ± 0.1 MPa. The FSC was placed in a heating-cooling stage (CAP500, Linkam) under the microscope of the Raman spectrometer. Temperature was controlled to ± 0.1 K.

Raman spectra acquisition

Raman spectra were acquired using a LabRAM HR spectrometer (Horiba Jobin-Yvon) equipped with a 600 gr.mm⁻¹ grating. Excitation was done by using the 514.53 nm line of an Ar⁺ laser at about 200 mW (Stabilite 2017, Spectra-Physics) and focused inside the capillary tube using a 20 \times objective (Olympus, N.A. = 0.4). Spectral resolution was about 1.6 cm⁻¹. A neon (Ne) lamp was positioned below the capillary to

record Ne emission line for wavelength calibration time to time. Neon reference lines were taken from the NIST Atomic Spectra Database^[33]. The Raman spectra were acquired at each P - T step after 20-30 min of equilibrium checked by a constant Raman signal. As previously done in our work on the solubility and diffusion of CO_2 ^[19] and CH_4 ^[16], measurements were done very close ($< 50\mu m$) to the liquid-gas interface. Each spectrum was the mean of 10 accumulations of 6-10 s. Six spectra were collected at each P - T step. The intensity of the signal of N_2 from the atmosphere was checked by recording a defocused Raman spectrum with the same parameters (laser power, objective, acquisition time).

Data processing

Experimental data were processed using Labspec 6 software (Horiba). A third-order polynomial baseline was subtracted between 1200 and 2000 cm⁻¹. Water bending vibration peak (~ 1640 cm⁻¹) and NO stretching vibration peak (~ 1867 cm⁻¹) were fitted using Gaussian-Lorentzian function to determine peak position, intensity (height), width (FWHM), and area (integrated intensity). Data acquisition and data processing were carried out by two different operators at different times (over more than 1 year) to ensure reproducibility. No difference between operators for data at similar P - T conditions was observed. The ratio between the peak area of NO and H_2O Raman signal (PAR: Peak Area Ratio) was selected as the most accurate parameter to follow NO solubility in water. Experimental uncertainty was calculated from the mean of the 6 repeated measurements. Uncertainty was expressed at 1σ .

Molecular simulation data sets at 295 K, 333 K and 373 K (see below for simulation method description) were each fitted using a second-order polynomial using Weighted Least Squares method to interpolate the data simulated at 4 different pressures to any pressure up to 60 MPa (LNE-RegPoly 1.0 software^[34]). Data from molecular simulations were then used to calculate the molar fraction of NO (x_{NO}) at all P steps of the experimental data in pure water at the same temperatures using LNE-RegPoly to propagate uncertainties.

A linear correlation between PAR and x_{NO} was then calculated using GLS-GGMR method to determine the fitting function considering uncertainty from PAR (experimental Raman uncertainty) and x_{NO} (simulation uncertainty). The experimental data at the same temperature as simulation (295 K, 333 K, and 373 K) were selected for calibration. The two data

points at higher pressure at 295 K were not included in calibration because of higher experimental uncertainty and the absence of such high-pressure points at other temperatures. x_{NO} for all experimental data in the fitting range (PAR range $\pm 10\%$) were finally determined using LNE-RegPoly to propagate uncertainties. x_{NO} values from PAR out of the fitting range were estimated simply applying the fitting function with no possibility to propagate uncertainty.

Simulation method

Monte Carlo method

The solubility of NO in water was also investigated by means of molecular simulation techniques which have been proven as valuable complementary approaches to experimental measurements, especially when hazardous compounds and/or extreme pressure or temperature conditions are considered. Monte Carlo (MC) simulations were performed in the Gibbs NPT ensemble (constant number of particles N , constant pressure P and constant temperature T) using the GIBBS Monte Carlo code^[35]. In such simulations, coexisting phases (in this study, a NO-rich phase and a H₂O-rich phase) were simulated in individual boxes without an explicit interface, and particle transfers between boxes were performed in order to ensure phase equilibrium. The following three MC move types were used in order to sample the configurational space of the studied systems: (i) internal moves (rigid body translations and rotations of a molecule), (ii) volume changes, (iii) transfers between phases using a pre-insertion bias^[36]. This pre-insertion bias algorithm, used to improve the efficiency of the sampling, involved two steps. The first step consisted in the selection of a suitable location for inserting a new molecule by testing several places with a simple Lennard-Jones particle. The second step involved the test of several orientations with the centre of mass of the inserted molecule at the location selected in the first step. The selected probabilities for the different MC move attempts were 0.3 for translations, 0.3 for rotations, 0.395 for transfers, and 0.005 for volume changes. A total number of 1000 water molecules and 100 NO molecules were considered in our MC simulations. For some conditions, simulations using a bigger system with 5000 water molecules were also performed in order to ensure that no size effect occurred. Three temperatures were investigated (295.15 K – 323.15 K – 373.15 K) for pressures ranging from 5–60 MPa. For each studied condition, a total number of at least $6 \cdot 10^8$ MC iterations were performed. Macroscopic fluid properties were

derived by calculating appropriate averages over generated configurations.

Interaction potentials and energy calculation

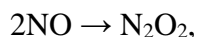
Nitric oxide and water molecules were represented using models proposed by Lachet et al.^[37] and Abascal and Vega^[38], respectively. In these models, molecules were considered to be rigid, thus no intramolecular energy was accounted for. Intermolecular energy was calculated with the two following contributions: dispersion-repulsion and electrostatic. Dispersion-repulsion energy between two force centres was represented as a function of their separation distance with a Lennard-Jones (LJ) potential. In the case of binary interactions involving different force centres, the Lorentz-Berthelot combining rules were used. Electrostatic energy was computed from the Coulomb law, assuming that the molecules bear electrostatic point charges. In the model proposed by Lachet et al.^[37], NO was treated as a single LJ sphere and the dipole moment of the molecule was neglected, thus no partial charges were considered for this molecule. H₂O was represented using the TIP4P/2005 model, *i.e.* a single LJ sphere located on the oxygen atom together with a distribution of three partial charges: two of them being located on the hydrogen atoms and the third one being shifted (0.1546 Å) from the oxygen nucleus toward an intermediate axial position. The distance between oxygen and hydrogen atoms was 0.9572 Å, and the HOH angle was 104.52 degrees. The force field parameters corresponding to these two models are presented in Table 1.

Calculation of this intermolecular energy was done by applying periodic boundary conditions, following classical procedures of molecular simulations^[39]. Lennard-Jones interactions were computed by applying a cut-off distance set to half of the box length. A standard long distance correction was used to account for interactions beyond the cut-off distance. The calculation of electrostatic interactions was done using the Ewald summation method with 7 vectors in each space direction and a Gaussian width set to $2\pi/L$, where L was the size of the simulation box.

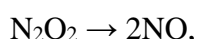
Nitric oxide dimerization study

Special attention must be paid when studying nitric oxide containing systems because this compound can exist as a mixture of monomers (NO: nitrogen monoxide) and dimers (N₂O₂: dinitrogen dioxide). The composition of the NO-N₂O₂ equilibrium mixture depends on pressure and temperature conditions: the dimer is favoured at high pressures and low temperatures^[40]. In order to assess the state of nitric oxide that must be considered in this study, a

monophasic *NPT* simulation of the reacting NO-N₂O₂ system was first conducted at 295.15 K and 60 MPa using reaction ensemble Monte Carlo (ReMC). The ReMC method^[41,42] allows the study of chemically reacting mixtures. During this simulation, an additional MC move, the reaction move, was used in order to account for the possible dimerization of two NO molecules into N₂O₂. This move consisted in firstly choosing a direction to perform the reaction, second in deleting a set of reactant molecules randomly chosen in the system, and finally inserting product molecules. In our case, the reaction move was:



where two randomly chosen NO molecules were deleted and one N₂O₂ was inserted, or



where one N₂O₂ molecule randomly selected was deleted and two NO molecules were inserted. To model N₂O₂ molecules, we used two NO LJ sites separated by 2.237 Å; the individual LJ parameters for each NO site in the dimer being the same as those for the monomer. No detailed description of these calculations is proposed here and we invite interested readers to investigate the two articles cited above^[41,42] for more details and the study of Lachet et al.^[37] for specific application of this method to nitric oxide study.

The simulation performed at 295.15 K and 60 MPa (*i.e.* the lowest investigated temperature and the highest investigated pressure of the present work) showed a mole fraction of dimers of 2.10⁻⁶. This result is consistent with our previous results conducted at lower pressures^[37] which showed that, for temperature above the critical temperature of the NO-N₂O₂ system ($T_c = 180.15$ K), associations fully disappeared. Only the monomer form of the nitric oxide (NO) was thus accounted for in this work.

Results

The Raman spectra of NO dissolved in water were recorded step by step at each pressure and temperature (Figure 1). The bending vibration mode of water is a large band around 1640 cm⁻¹^[43]. The main peak of dissolved NO is visible at 1868 cm⁻¹ (symmetric stretching). No literature data refereeing to the Raman spectrum of dissolved NO was found so the assignment was done by comparison with the position of the gaseous species at 1877 cm⁻¹^[44,45]. The only other species is N₂ with a signal of the same intensity as the one found in the atmosphere (2331 cm⁻¹).

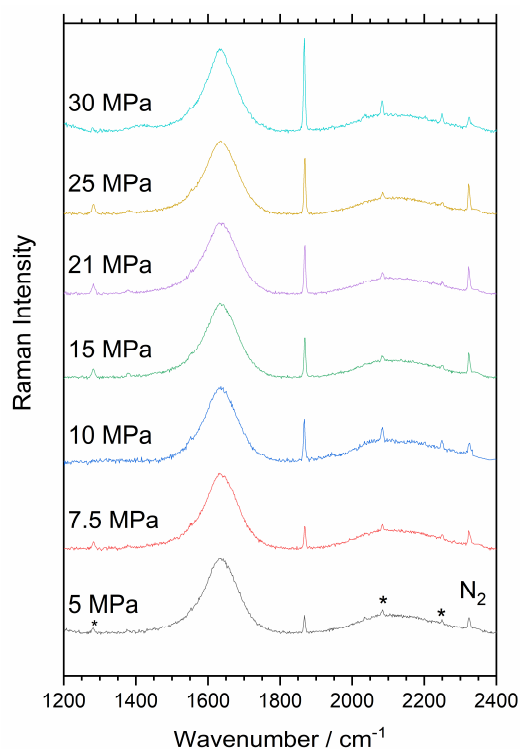


Figure 1. Raman spectra of NO dissolved in liquid water at 298 K as a function of pressure. N₂ is from the air. * Ne lamp

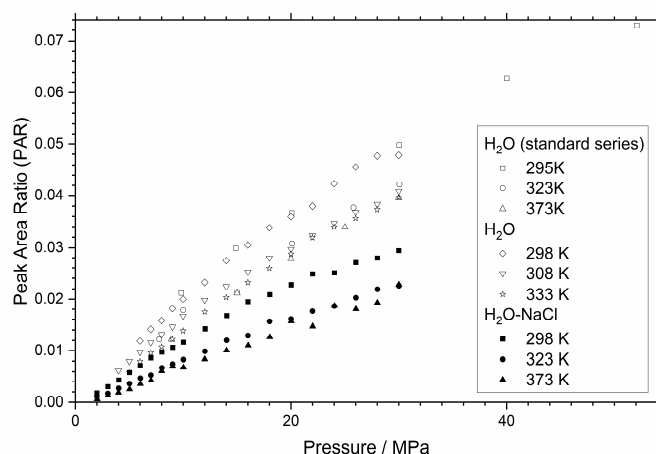


Figure 2. PAR as a function of pressure, at different temperatures for NO in pure water (standard series used for calibration based on simulation data) and brine (1M-NaCl-H₂O). Error bars are not shown because they are smaller than symbol size.

The intensity of the signal of NO increases when pressure increases (**Erreur! Source du renvoi introuvable.**). Peak position and shape are constant. Temperature does not affect band shape and band position (not shown here). Traces of the oxidized species were detected in some cases at the end of the experiments, with signals corresponding to nitrate (at 1041 cm⁻¹ and 1410 cm⁻¹). The PAR calculated from Raman data were plotted as a function of pressure, temperature and salinity (Figure 2). The PAR increases when pressure increases. PAR decreases

when temperature increases. It means that NO solubility decreases from 295 K to 373 K. For the same temperature and pressure, PAR decreases when NaCl is added, i.e. NO solubility is affected by a salting out effect.

To calculate solubility from PAR, the experimental PAR data are calibrated on simulation data giving NO solubility as a function of pressure at 295 K, 323 K and 373 K (Figure 3) as there is only a few experimental data available in the literature and only at atmospheric pressure^[8–12]. As observed on Raman data, the solubility of NO increases when pressure increases and decreases from 295 K to 373 K.

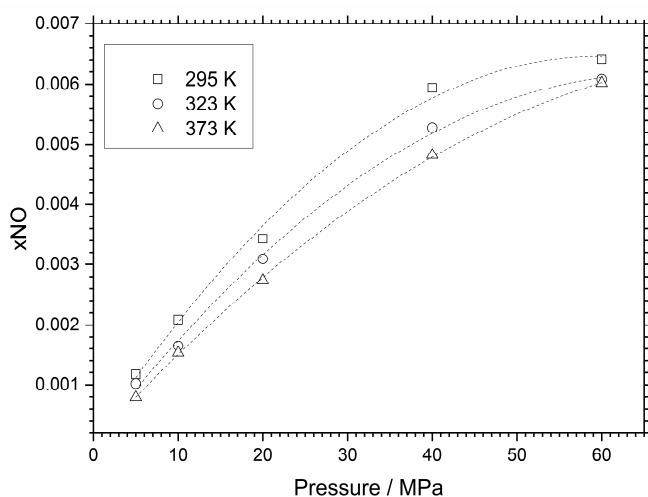


Figure 3. Simulation data of NO solubility (molar fraction, x_{NO}) in pure water as a function of pressure and temperature.

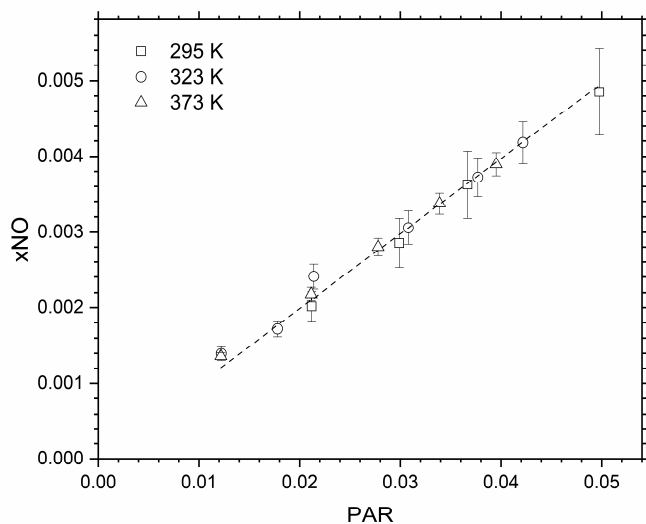


Figure 4. NO solubility (molecular simulation data) vs. PAR (Raman).

Molecular simulation data of x_{NO} in pure water (Table 2) were interpolated by a polynomial function for each temperature in order to determine NO solubility at any pressure. A unique linear correlation

(1) was established between simulation data and all experimental Raman data at 295 K, 323 K and 373 K in pure water (Figure 4) as no temperature effect can be observed in the investigated ranges of P and T conditions. Based on previous studies, it was also supposed that low salinity (1 M) does not significantly affect the calibration line slope^[17,46–48] below 373 K.

$$x_{\text{NO}} = 0.09927 \text{ PAR} \quad R^2 = 0.999 \quad (1)$$

Based on the relation derived from Figure 4, the Raman data in Figure 2 were then converted into molar fraction scale at all temperatures in pure water and in saline solutions (Figure 5). All numerical data are gathered in Table S1.

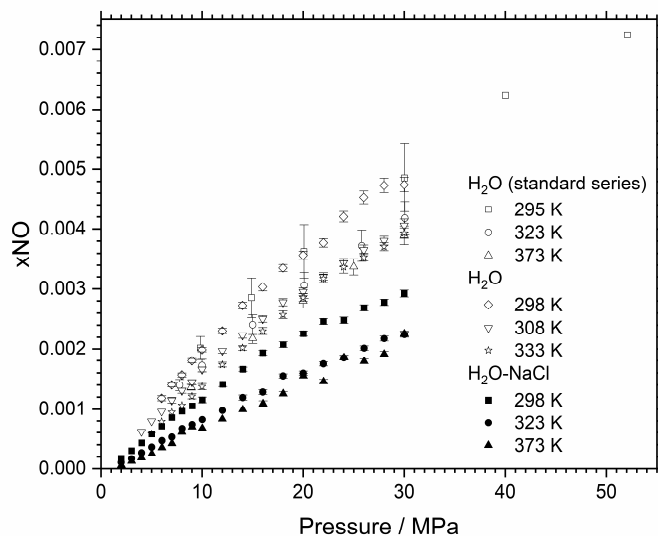


Figure 5. Solubility of NO (molar fraction, x_{NO}) in water (standard series are the ones used for calibration from molecular simulations, Figure 4) and brine (1M-NaCl-H₂O) as a function of pressure and temperature, from Raman data. Error bars were calculated by propagation of PAR uncertainty and from the uncertainty of the GLS-GGMR fitting in Figure 4. Data provided in Table S1.

Discussion

The Raman peak area of one vibration mode of a molecule is proportional to the number of molecules in the analysed volume^[49]. It means that the peak area ratio is proportional to concentration (moles per litre of solution). The linearity of this relation may be affected by a variation of the refractive index of the solution or of the cross-section (efficiency) of the considered vibration mode^[50]. The linearity observed in Figure 4 demonstrated that these effects can be neglected in the PTX range of these experiments.

The dissolution of NO in an aqueous solution follows the same rule as other non-polar gases (CH₄, N₂, O₂,

CO,...), i.e. an increase of solubility with pressure, a decrease of solubility with temperature between 295 K and 373 K then solubility increases at higher temperature^[10,51]. Solubility decreases when salinity increases^[12] (salting out effect). This last point is in agreement with literature at room pressure^[12].

No other species than dissolved NO was detected in the Raman spectra. Despite careful preparation of the samples and evacuation under vacuum of all the experimental setup before loading gas, oxidized ions (nitrate) appear in some cases at the end of the experiments. It could be due to the reaction of NO with residual gaseous O₂ in the experimental device or dissolved O₂ in water or due to NO disproportionation. Disproportionation reactions of NO to give NO₂ and N₂O were described at high pressure^[52] or in the presence of catalyser^[53] but should not occur in the investigated ranges of pressure and temperature. It was therefore considered that the main process generating oxidized species in these experiments was oxidation by residual O₂.

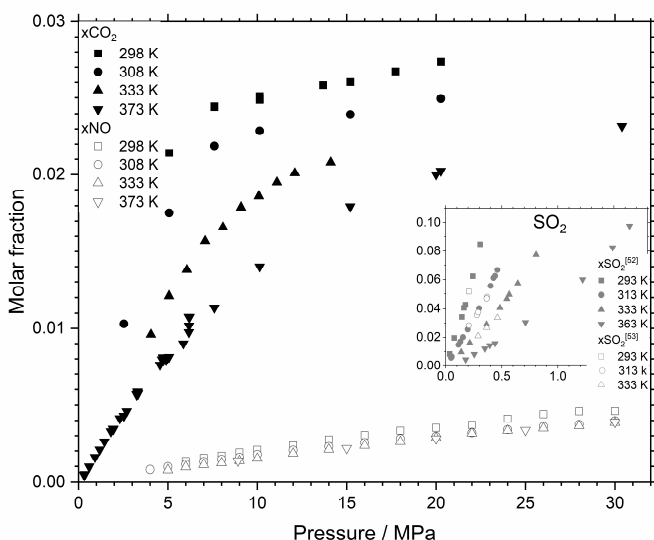


Figure 6. Comparison of NO, SO₂ and CO₂ solubility in water as a function of pressure and temperature. Solubility data are from Rumpf et Maurer^[55] and Zhou et al.^[30] for SO₂ and from Corvisier et al.^[54] and references therein for CO₂.

The solubility of NO in pure water determined in this study was compared to experimental data of CO₂ and SO₂ solubility from literature^[30,54,55] (Figure 6). NO is about 5-15 times less soluble than CO₂ in pure water. The effect of pressure and temperature are similar but a change in the solubility slope curve is observed for CO₂ at intermediate pressure (especially at low temperature). The CO₂ behaviour could be linked to a change of CO₂ from gas-like to liquid-like compound over critical temperature T_c whereas the T_c of NO is far from the studied temperature range (180 K). SO₂ is quite more soluble than CO₂ by about one order of

magnitude and thus is about 50 to 100 times more soluble than NO at low pressure (<1.7 MPa). There is no reliable solubility data of SO₂ at higher pressure^[30,54] in this range of temperature because of complex phase changes.

Conclusion

For the first time, the solubility of NO under geological conditions of pressure and temperature was determined using a coupled approach of Raman spectrometry and Monte Carlo molecular simulation. The extrapolation of the range of calibration by simulation was possible in the limit of the linearity of the correlation between Raman data and simulation, at least in the range 295-373 K, 2-60 MPa and 0-1 M-NaCl-H₂O. No chemical reaction was observed, NO being stable in the experimental ranges of P and T conditions for the time of the experiments. The new data of solubility in aqueous solutions can be used to fit standard equations of state and to implement the geochemical codes used to simulate water/gas/rock interactions in the case of the geological storage of CO₂ with SO_x-NO_x impurities.

These reactive gases found as impurities in fumes that could be stored underground in CCS projects show specific and different behaviours as a function of pressure, temperature and salinity. The understanding and thus the prediction of the behaviour of such complex mixtures will be addressed only if the thermodynamic properties of such gases are well known under the geological conditions of storage.

For that, the FSC technique appears as the more suitable technique to meet this challenge. The experimental device will be used in further studies to measure solubilities in extended ranges of pressure, temperature and salinity for pure gases but also for gas mixtures of non-reactive and reactive compounds such as CO₂, NO, NO₂, N₂O or SO₂, controlling phase transitions by optical microscopic observations as well as chemical speciation and equilibria by Raman spectroscopy.

Acknowledgments

This work was supported by the ANR grants (“GazAnnexes” ANR-06-CO2-005 and “SIGARRR” ANR-13-SEED-0006), INSU CESSUR grant and Carnot Institute Ic el.

This is the peer reviewed version of the following article: Sterpenich, J., Caumon, M.-C., Lachet, V., Creton, B., Jarmouni, M.E., Randi, A., Robert, P., 2021. NO solubility in water and brine up to 60 MPa and 373 K by combining Raman spectroscopy and molecular simulation. Journal of Raman

Spectroscopy 1–9, which has been published in final form at <https://doi.org/10.1002/jrs.6072>. This article may be used for non-commercial purposes in accordance with Wiley Terms and Conditions for Use of Self-Archived Versions.

References

- [1] IEAGHG, *Effects of impurities on geological storage of CO₂*, **2011**.
- [2] J. Sterpenich, J. Dubessy, J. Pironon, S. Renard, M.-C. Caumon, A. Randi, J.-N. Jaubert, E. Favre, D. Roizard, M. Parmentier, M. Azaroual, V. Lachet, B. Creton, T. Parra, E. E. Ahmar, C. Coquelet, V. Lagneau, J. Corvisier, P. Chiquet, *Energy Procedia* **2013**, *37*, 3638.
- [3] J. Corvisier, A.-F. Bonvalot, V. Lagneau, P. Chiquet, S. Renard, J. Sterpenich, J. Pironon, *Energy Procedia* **2013**, *37*, 3699.
- [4] P. N. Seevam, J. M. Race, M. J. Downie, P. Hopkins, in *2008 7th International Pipeline Conference*, American Society of Mechanical Engineers Digital Collection, **2008**, pp. 39–51.
- [5] H. Liu, Y. Shao, *Appl. Energy* **2010**, *87*, 3162.
- [6] J. Wang, D. Ryan, E. J. Anthony, N. Wildgust, T. Aiken, *Energy Procedia* **2011**, *4*, 3071.
- [7] B. Creton, V. Lachet, *Thermodynamic Study of Binary Systems Containing Carbon Dioxide and Associated Gases Using Molecular Simulation Techniques*, Social Science Research Network, Rochester, NY, **2019**.
- [8] J. N. Armor, *J. Chem. Eng. Data* **1974**, *19*, 82.
- [9] L. W. Winkler, *Eur. J. Inorg. Chem.* **1901**, *34*, 1408.
- [10] J. A. Dean, N. A. Lange, Eds., *Lange's handbook of chemistry*, McGraw-Hill, New York, NY, 15. ed., **1999**.
- [11] I. G. Zacharia, W. M. Deen, *Ann. Biomed. Eng.* **2005**, *33*, 214.
- [12] A. E. Markham, K. A. Kobe, *J. Am. Chem. Soc.* **1941**, *63*, 449.
- [13] J. Corvisier, I. Sin, *Considering Non-Ideal Gas Mixtures in Geochemical Modeling of Gas-Water-Salt-Rock Interactions: Application to Impure CO₂ Geological Storage*, Social Science Research Network, Rochester, NY, **2019**.
- [14] I.-M. Chou, in *Raman Spectroscopy Applied to Earth Sciences and Cultural Heritage*, (Eds: J. Dubessy, M.-C. Caumon, F. Rull), The European Mineralogical Union and the Mineralogical Society of Great Britain, London, **2012**, vol. 12, pp. 227–247.
- [15] I. M. Chou, R. C. Burruss, W. Lu, in *Advances in High-Pressure Technology for Geophysical Applications*, (Eds: J. Chen, Y. Wang, T. S. Duffy, G. Shen, L. F. Dobrzhinetskaya), Elsevier, Amsterdam, **2005**, pp. 475–485.
- [16] M.-C. Caumon, P. Robert, E. Laverret, A. Tarantola, A. Randi, J. Pironon, J. Dubessy, J.-P. Girard, *Chem. Geol.* **2014**, *378–379*, 52.
- [17] M.-C. Caumon, J. Dubessy, P. Robert, B. Benaissa, *Energy Procedia* **2017**, *114*, 4843.
- [18] W. Lu, I. M. Chou, R. C. Burruss, *Geochim. Cosmochim. Acta* **2008**, *72*, 412.
- [19] C. Belgodere, J. Dubessy, D. Vautrin, M.-C. Caumon, J. Sterpenich, J. Pironon, P. Robert, A. Randi, J.-P. Birat, *J. Raman Spectrosc.* **2015**, *46*, 1025.
- [20] W. J. Lu, I. M. Chou, R. C. Burruss, M. Z. Yang, *Appl. Spectrosc.* **2006**, *60*, 122.
- [21] W. J. Lu, H. R. Guo, I. M. Chou, R. C. Burruss, L. L. Li, *Geochim. Cosmochim. Acta* **2013**, *115*, 183.
- [22] J. Fang, I.-M. Chou, Y. Chen, *J. Raman Spectrosc.* **2018**, *49*, 710.
- [23] V.-H. Le, M.-C. Caumon, A. Tarantola, P. Robert, A. Randi, in *XIII GeoRaman*, Catania, Italy, **2018**, p. 96.
- [24] A. Fall, B. Tattitch, R. J. Bodnar, *Geochim. Cosmochim. Acta* **2011**, *75*, 951.
- [25] H. M. Lamadrid, Leeds, UK, **2015**, p. 90.
- [26] L. Shang, I.-M. Chou, R. C. Burruss, R. Hu, X. Bi, *J. Raman Spectrosc.* **2014**, *45*, 696.
- [27] M. Wang, I.-M. Chou, W. Lu, B. D. Vivo, *Eur. J. Mineral.* **2015**, *27*, 193.
- [28] H. Guo, Y. Chen, Q. Hu, W. Lu, W. Ou, L. Geng, *Fluid Phase Equilibria* **2014**, *382*, 70.
- [29] L. Jiang, Y. Xin, I.-M. Chou, Y. Chen, *J. Raman Spectrosc.* **2018**, *49*, 343.
- [30] Q. Zhou, H. Guo, P. Yang, Z. Wang, *Ind. Eng. Chem. Res.* **2020**, *59*, 12855.
- [31] V.-H. Le, M.-C. Caumon, A. Tarantola, A. Randi, P. Robert, J. Mullis, *Anal. Chem.* , DOI:10.1021/acs.analchem.9b02803.
- [32] V.-H. Le, M.-C. Caumon, A. Tarantola, A. Randi, P. Robert, J. Mullis, *Chem. Geol.* **2020**, *552*, 119783.
- [33] A. Kramida, Yu. Ralchenko, J. Reader, and NIST ASD Team, NIST Atomic Spectra Database (ver. 5.7.1), (accessed 6 December 2019).
- [34] C. Yardin, in *16th International Congress of Metrology*, (Eds: J.-R. Filtz, B. Larquier, P. Claudel, J.-O. Favreau), EDP Sciences, Paris, France, **2013**, p. 04009.
- [35] P. Ungerer, B. Tavitian, A. Boutin, *Applications of molecular simulation in the oil*

- and gas industry: Monte Carlo methods*, Editions Technip, **2005**.
- [36] E. Bourasseau, P. Ungerer, A. Boutin, *J. Phys. Chem. B* **2002**, *106*, 5483.
- [37] V. Lachet, B. Creton, T. De Bruin, E. Bourasseau, N. Desbiens, Ø. Wilhelmsen, M. Hammer, *Fluid Phase Equilibria* **2012**, *322*, 66.
- [38] J. L. Abascal, C. Vega, *J. Chem. Phys.* **2005**, *123*, 234505.
- [39] M. P. Allen, D. J. Tildesley, *Computer simulation of liquids*, Oxford university press, **2017**.
- [40] A. Snis, I. Panas, *Chem. Phys.* **1997**, *221*, 1.
- [41] W. R. Smith, B. Triska, *J. Chem. Phys.* **1994**, *100*, 3019.
- [42] J. K. Johnson, A. Z. Panagiotopoulos, K. E. Gubbins, *Mol. Phys.* **1994**, *81*, 717.
- [43] G. E. Walrafen, *J. Chem. Phys.* **1964**, *40*, 3249.
- [44] D. G. Fouche, R. K. Chang, *Appl. Phys. Lett.* **1972**, *20*, 256.
- [45] C. M. Penney, L. M. Goldman, M. Lapp, *Nature* **1972**, *235*, 110.
- [46] M.-C. Caumon, J. Sterpenich, A. Randi, J. Pironon, *Int. J. Greenh. Gas Control* **2016**, *47*, 63.
- [47] M.-C. Caumon, J. Sterpenich, A. Randi, J. Pironon, *Energy Procedia* **2017**, *114*, 4851.
- [48] X. Wu, W. Lu, W. Ou, M.-C. Caumon, J. Dubessy, *J. Raman Spectrosc.* **2017**, *48*, 314.
- [49] G. Placzek, *The Rayleigh and Raman Scattering*, Lawrence Radiation Laboratory, **1959**, vol. 526.
- [50] H. W. Schrötter, H. W. Klöckner, in *Raman Spectroscopy of Gases and Liquids*, (Ed: A. Weber), Springer Berlin Heidelberg, Berlin, **1979**, vol. 11, pp. 123–166.
- [51] J. Zheng, S. Mao, *Appl. Geochem.* **2019**, *107*, 58.
- [52] S. F. Agnew, B. I. Swanson, L. H. Jones, R. L. Mills, *J. Phys. Chem.* **1985**, *89*, 1678.
- [53] G. G. Martirosyan, A. S. Azizyan, T. S. Kurtikyan, P. C. Ford, *Inorg. Chem.* **2006**, *45*, 4079.
- [54] J. Corvisier, C. Coquelet, E. El Ahmar, J. Sterpenich, L. Richard, R. Privat, J.-N. Jaubert, J.-Y. Coxam, K. Ballerat-Busserolles, P. Cézac, F. Contamine, V. Lachet, B. Creton, M. Parmentier, L. André, P. Blanc, L. de Lary, A. Lassin, J. Tremosa, E. Gaucher, *Rapport bibliographique pour les systèmes eau-gaz-sel d'intérêt pour le projet SIGARRR*, **2014**.
- [55] B. Rumpf, G. Maurer, *Fluid Phase Equilibria* **1992**, *81*, 241.

Table 1. Force field parameters (σ and ϵ represent the diameter and the energetic parameter of the LJ potential, respectively and q^- stands for the point charge) used to mimic NO and H₂O molecule's behaviour.

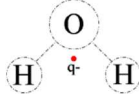
Molecule	Force center or charge	σ (Å)	ϵ (K)	q (e)	Ref.
	NO	3.4000	130.0000	---	Lachet, 2012
	O	3.1589	93.1990	---	Abascal, 2005
	H	---	---	0.5564	
	q^-	---	---	-1.1128	

Table 2. Molar fraction of NO (x_{NO}) in water as a function of pressure and temperature from molecular simulation calculations

Temperature / K	Pressure / MPa	x_{NO} ($\times 10^3$)	$u(x_{NO})$ ($\times 10^3$)
295	5	1.2	0.3
	10	2.1	0.3
	20	3.4	0.7
	40	5.9	1.1
	60	6.4	0.9
333	5	1.02	0.12
	10	1.65	0.14
	20	3.1	0.4
	40	5.3	0.5
	60	6.1	0.9
373	5	0.79	0.05
	10	1.53	0.07
	20	2.74	0.19
	40	4.8	0.3
	60	6.0	0.5

Table S1. NO solubility (molar fraction x_{NO}) in pure water and 1M NaCl solution calculated from Raman data. Data in italic are extrapolated out from the initial calibration range.